Elastic electron scattering from ortho-, meta-, and paraxylenes, C_{8}H_{10}

A. Sakaamini, S. M. Khakoo, L. Hargreaves, M. A. Khakoo, D. F. Pastega, and M. H. F. Bettega

Phys. Rev. A **95**, 022702 — Published 2 February 2017

DOI: 10.1103/PhysRevA.95.022702

Elastic electron scattering from ortho-, meta- and para-xylenes, C_8H_{10}.

A. Sakaamini[1,3], S. M. Khakoo[1], L. Hargreaves[1], M. A. Khakoo[1], D. F. Pastega[2] and M. H. F. Bettega[2]

[1] Physics Department, California State University, Fullerton, CA 92831, USA.

[2]Departamento de Física, Universidade Federal do Paraná, Caixa Postal 19044, 81531-990 Curitiba, Paraná, Brazil.

[3]Present Address: The School of Physics and Astronomy, The University of Manchester, Manchester, M13 9PL, United Kingdom

ABSTRACT:*Ab intio* calculations and normalized experimental measurements of the differential and integral cross sections for vibrationally elastic scattering of low-energy electrons from ortho-xylene, meta-xylene and para-xylene are presented. The calculated cross sections are obtained using the Schwinger multichannel method implemented with norm-conserving pseudopotentials. The differential cross sections are measured at incident energies from 1 eV to 30 eV and scattering angles from 10^o to 130^o. These cross sections are compared to experimental results for toluene. The comparisons illuminate the role of molecular structure in determining the integral cross sections and the angular distributions of resonantly scattered electrons.

PACS number(s): 34.80.Bm, 34.80.Gs

1. Introduction

Interest in collisions of low-energy electrons with gaseous aromatic polyatomic molecules was brought up by the seminal electron attachment work of [1] which concerned breakup of C=C bonds in these compounds by low energy electrons in the form of π^* resonances. Of interest is the study of variations of ring aromatics (e.g. furans) found in organic systems such as DNA, whose most commonly encountered aromatic compound is benzene. Replacing one H-atom by a methyl group to form toluene breaks the D_{6h} symmetry of benzene. The symmetry breaking lifts the degeneracy of the two lowest occupied π orbitals in the C-atom, which in turn shifts the energy of the negative ion resonances formed by electron attachment [2,3] as well as increases the cross section for electron attachment [4,5]. Our group recently measured low energy elastic scattering differential cross sections (DCS) from toluene [6], and compared our results with existing DCSs of Kato *et al.* [7] and found mostly good agreement with their results. Comparison of our toluene DCS with those of Cho *et al.* [8] for benzene, revealed that the toluene DCSs were in most cases significantly higher than those of benzene by about 20% for the same incident energy (E_0) values.

As planned in our project to look at aromatic compounds, we decided to measure DCSs for elastic electron scattering from xylene isomers (see Fig. 1). By comparing cross sections of xylene isomers with each other and also with the cross sections of toluene and benzene, we want to investigate the effect of methylation in the resonance spectra of xylenes isomers. We note that the investigation of methylation in smaller systems can bring some insight of what happens in larger systems, in particular DNA, where this effect is important in gene regulation and other mechanisms [9].

Isomeric differences in compounds in terms of have been of great interest in medical research, especially in the case of stereoisomers, which react differently with DNA. From the present

perspective, isomers which have significant differences in geometric structure and therefore physical properties (viz. electric moments) should have differences in their dynamics with regards to interaction with scattering particles such as electrons, and photons. An example of such work was done by Zhou *et al.* [10], for photoionization of ortho-, meta- and para- xylenes. They found the three isomers behaved similarly, however since their work is not differential in angle, we expect that it is possible to see differences between these isomers for differential electron scattering from these isomers. A quite complete survey on electron and positron collisions with isomers of hydrocarbons and isomers of other molecules can be found in [11].

In addition, electron impact on hydrocarbons has recently become a research topic in long term electric propulsion of space vehicles using massive particle where low cost alternatives for xenon (currently the fuel of choice, mass 131 amu.) could be replaced by hydrocarbons such as inert cage-type "diamondoid" hydrocarbons e.g. adamantane ($C_{10}H_6$, 136 amu.) [12]. Presently, xylene (106 amu.) is a constituent of liquid fuels such as jet fuel and so combustion studies of it induced by electrical sparking is of interest especially in the orientation of the $-CH_3$ groups on the benzene ring and its ionization to provide fuels for space vehicles may also be an option.

Ortho-xylene has been shown to possess a much greater degree of reactivity towards oxygen than its isomers meta- and para-xylene [13]. Under identical conditions, it exhibits a maximum reaction rate of the order of ten times that observed for the less reactive isomers. Xylene isomers are considered volatile organic compounds, which are regularly emitted in the exhaust gases of paint factories, production of semiconductors and production and/or transport of liquid fuels. The removal of these from gaseous effluents is dependent on the pollutant nature, its concentration and amount of gas effluent. One of the most recommended methods for removal is the catalytic combustion [14]. In all these cases, electron interaction with the target (attachment, dissociation,

ionization) is a major route to cause its degradation. There is very little work done on the electron scattering from xylene isomers. The residual energy electron spectra of all isomers of xylene were taken at 3eV above threshold by Yamamoto *et al.* [15]. They found all three isomers were essentially identical with only minor differences. Inner shell excitation of the C 1s orbital was made by Eustatiu *et al.* [16], who observed very similar spectra for all three isomers. Similar observations for the total ionization cross section of the isomers of xylene was made by Jiao and Adams [17] who find the same total electron impact ionization cross sections for all three isomers from threshold to 200 eV. They found m-xylene having a somewhat larger cross section, with o-xylene being the lowest. Unfortunately these differences were all within the error uncertainties of their measurements. Also, their results are in very good with the result of Harrison *et al.* [18] at the E_0 of 75 eV. They also investigated the major product ions produced of which the single ionization of C_8H_{10} to produce $C_8H_{10}^+$ had the largest cross section.

Studying all three isomers would reveal the importance of the physical structure as regards the variation in symmetry in the positioning of the two CH_3 radical groups around the benzene ring, and in particular see how significantly it affects the scattering cross section as well as the position of the negative ion resonance dynamics for such a large target, i.e. how much the overall size of the target relative to the CH_3 radicals affected the cross sections. Whereas the dipole polarizabilities of these isomers are similar i.e. around the same value of ≈ 16 Å^3 [19], the three isomers, shown in Fig. 1, have differences in their permanent dipole moments. Here p-xylene, m-xylene and o-xylene have increasing dipole moments of 0.02 D, 0.30 D and 0.45D [20].

In the present work, we present differential, integral and momentum transfer cross sections for o-xylene, m-xylene and p-xylene. For all these targets we have conducted a joint experimental and theoretical study to provide low energy differential elastic and integral cross sections, and to

compare our results between the theory and experiment. To calculate the cross sections we employed the Schwinger multichannel method with pseudopotentials, in the static-exchange plus polarization approximation.

In the following, we describe in Sec. II the experimental and theoretical methods used in this work. In Sec. III we present our results and the comparisons between the isomers and toluene cross sections along with discussions about the results. In Sec. IV we finalize with our overall conclusions. In this work our DCSs were taken at E_0 values of 1.0eV, 1.5 eV, 2.0eV, 3.0eV, 5.0eV, 10.0 eV, 15.0eV, 20.0eV and 30.0eV and scattering angles (θ) from 10^o to 130^o.

IIa. Experimental

Our experimental setup is detailed in e.g. Khakoo *et al*. [21]. The electron gun and detector employed double hemispherical energy selectors, and the apparatus was made of titanium. Cylindrical lenses were used to transport scattered electrons through the system, which was baked to about 130^o with magnetically free biaxial heaters [22]. Electrons were detected by a discrete dynode electron multiplier [23] with a dark count rate of <0.01Hz and capable of linearly detecting $>10^5$ Hz without saturating. The remnant magnetic field in the collision region area was reduced to ≈1mG at the collision region by a double μ-metal shield. Typical electron currents were around 18-25 nA, with an energy resolution of between 40-70 meV, full-width at half-maximum. Lower currents were chosen for lower E_0 values to counter space charge broadening of the incident electron beam. The electron beam could be easily focused at 1 eV and remained stable, varying less than 15% at maximum during the data acquisition period. The energy of the beam was established by repetitively (at least daily) measuring the minimum in the elastic scattering of the 2^2S He^- resonance at 19.366 eV [24] at $\theta = 90^o$ to about ≈40meV stability during a daily run.

Typically the contact potential varied from 0.6 eV to 0.7 eV. Energy loss spectra of the elastic peak were collected at fixed E_0 values and θ by repetitive, multi-channel-scaling techniques. The effusive target gas beam was formed by flowing gas through a 0.3mm diameter aperture, which was sooted (using an acetylene flame) to reduce secondary electrons. In using the aperture instead of a conventional tube gas collimator, we obviate the experimental need to maintain the gas pressures of the target gases in an inverse ratio of their molecular diameters, thus removing an additional systematic source of error that could occur in using tube collimators or similar, see e.g. [25]. This is a great advantage when working with large molecular targets of masses greater than 100 a.m.u. since the uncertainty in the molecular diameters of such targets can be considerable and applying the inverse molecular diameter ratio accurately in the Relative Flow Method is made more challenging, also with the stability of flow of these large targets through collimating needle sources. The aperture, located ≈7mm below the axis of the electron beam, was incorporated into a moveable source [25, 26] arrangement. The moveable gas source method determines background electron-gas scattering rates expediently and accurately [26]. The measured DCSs were normalized using the Relative Flow Method with helium as the reference gas, using DCSs from the well-established work of Nesbet [27] for E_0 below 20eV and of Register *et al*. [28] for E_0 above 20eV. The pressures behind the aperture ranged from 1.2 to 2 torr for He and 0.06 to 0.1 torr for toluene, resulting in a chamber pressure ranging from 1.0×10^{-6} torr to 2×10^{-6} torr. Xylene has a high molecular mass (106.2 a.m.u.) and is the heaviest target so far used in our system. Similar to tolueneits high viscosity caused instabilities in the flow as it blocked our gas bleed valve (Granville-Phillips Series 203 valve, [29]) and necessitated its baking at a temperature of about 60-70 ^{o}C. Also, the entire gas line after the bleed valves was heated to ≈ 84 ^{o}C to prevent condensation of xylene. Each DCS was taken a minimum of two times to check its reproducibility

and weighted averaging was made of multiple data sets to obtain the final DCSs. Integral cross sections (ICS) and Momentum Transfer Cross Sections (MTCS) were evaluated from the measured DCS by extrapolating the DCS to $\theta = 0^o$ and 180^o as described in [30] and numerically integrating the extrapolations using a spline fit.

IIb. Theoretical

In order to compute the cross sections for the xylene isomers we employed the Schwinger multichannel method (SMC) [31], implemented with norm-conserving pseudopotentials (SMCPP) [32] and parallel processing [33]. The SMCPP is a well-established method and a review of this method can be found in reference [34]. In this section we only discuss the theoretical aspects that are related to the present calculations.

The scattering calculations were performed at the equilibrium geometry of the targets ground state as obtained from a density functional theory (DFT) with B3LYP functional and aug-cc-pVDZ basis set, as implemented in the package GAMESS [35]. The xylene isomer exists in different conformations, which belong to different symmetry groups depending of the orientation of the methyl group in each isomer. At the ground state, o-xylene and p-xylene belongs to C_{2v} [36] point group, while m-xylene belongs to C_S point group. The optimized structures of the xylene isomers are shown in Fig. 1. In the scattering calculations, for carbon atoms, we employed a 6s5p1d Cartesian Gaussian functions (generated according to [37]) to represent the valence electrons, as the core electrons were replaced by the pseudopotentials of Bachelet *et al.* [38]. For the hydrogen atoms we employed the $4_S/3_S$ basis set of Dunning [39] augmented with one *p*-type function with exponent equal to 0.75. At this level of calculation, we found the dipole moment values of 0.06, 0.36 and 0.63D for p-xylene, m-xylene and o-xylene respectively.

Our calculations were carried out in the static-exchange (SE) and in the static-exchange plus polarization (SEP) approximations. We will present only our results obtained in the SEP approximation. In the SE and SEP approximations the scattering wave function is expanded in a set of configurations-state functions (CSFs). For the SE level of approximation the CSFs were build as $|\chi_{ij}\rangle = \mathrm{A}[|\Phi_0\rangle \otimes |\varphi_j\rangle]$, while in the SEP level of approximation the CSFs space is augmented with configurations generated as $|\chi_{ij}\rangle = \mathrm{A}[|\Phi_i\rangle \otimes |\varphi_j\rangle]$, where $|\Phi_0\rangle$ is the target ground state, $|\Phi_i\rangle$ is a singly excited virtual target state, $|\varphi_j\rangle$ is a single-particle function representing the scattering orbital, and A is the antisymetrizer. To represent the scattering and particle orbitals, we employed modified virtual orbitals (MVOs) [40], as generated in the field of a cationic Fock operator with charge +6. We present our calculations in the SEP approximation where the CSF space was formed by doublets obtained from singlet and triplet coupled excitations of the target. These virtual excitation were taken from all valence orbitals to the 40 lowest MVOs. We obtained 21751 CSFs for o-xylene and p-xylene (5600 in A_1, 5378 in A_2, 5430 in B_1 and 5574 in B_2) and 20832 CSFs for m-xylene (10790 in A′ and 10042 in A′′). We also employed the standard Born-closure procedure [41] to account for scattering of higher partial waves due the long-range character of the dipole potential of the target, since our scattering calculations only adequately describes the lower partial waves.

III. Results and Discussion

Our experimental DCSs are listed in Table 1 along with standard deviation errors determined from statistics of the background subtracted scattered electron counts, DCS reproducibility, and estimated errors in gas flow-rates (2% for He and 3% for xylene) and in the helium elastic DCSs (5 to 7%) used for normalization of the xylene DCSs.

Our experimental and calculated DCSs are plotted in Fig. 2 along with the DCSs for toluene [6]. "Excitation functions" of DCSs for elastic scattering at 90^o are presented in Fig. 3, while the ICSs and MTCSs are shown in Fig. 4. We present comparisons of the present DCSs with those of toluene taken earlier by our group [6] and those by Cho *et al.* [8] at E_0 = 30 eV. For toluene, at energies of $E_0 \geq 5$ eV agreement between the DCSs from [6] and [8] is very good. For E_0 = 1 eV the toluene DCS is mostly forward peaked due to the permanent dipole moment of the molecules, whereas that of all three xylenes are somewhat similar in the backward scattering region, with m-xylene and p-xylene showing some forward scattering for $\theta \geq 30^o$. At this energy, p-xylene shows essentially isotropic behavior typical of a molecule with a small dipole moment. In fact, all molecules present small dipole moment and this is reflected in the forward peaked behavior of the DCSs, which occurs at small scattering angles. The dipole polarizabilities of these molecules, around 16Å^3, have similar values of 12.31Å^3 and 10.33 Å^3 [42,43] for toluene and benzene, respectively, and so this forward scattering behavior seems to be due more to the permanent dipoles of these molecules then their polarizabilities. Besides, this energy is close to the 1 eV π_1* resonance (see Table 3) which in the DCS for m-xylene and o-xylene shows more of a p-type angular distribution than p- xylene. This is confirmed by theory, which shows this resonance for p-xylene to be too low in energy (at E_0 = 0.78 eV, see Table 3). This near-1 eV resonant behavior is somewhat alluded to our $\theta = 90^o$ excitation functions which rise around this energy, but unfortunately the experimental data does not extend below 1eV. Nevertheless, it is possible using our theoretical results to observe with some more detail in Fig. 5, that the first π_1* shape resonance occurs in different positions with respect to the different isomers. While for p-xylene the first resonance is located at 0.78 eV, m-xylene and o-xylene have the first resonance located at 1.00 and

1.10 eV respectively. This fact can explain the differences seen in the DCSs of the two isomers at this particular energy.

At E_0 = 1.5 eV, the three xylenes display essentially identical within error bars. Here, a comparison with toluene shows a similar angular distribution, but toluene is about a factor of 1.8 lower. This difference makes up for quite a large contribution due to the addition of a single methyl group to a benzene ring, but is reasonable when one considers roughly the geometric added radius of the group (about 33% greater, this does account roughly for the increased cross section). This ratio of cross section is found at most of the E_0 values. At E_0 = 2.0 eV we observe the xylene DCSs having similar qualitative and quantitative behavior. At E_0 = 3.0 eV, the o-xylene DCS is significantly different at $\theta \geq 80^o$, showing a different angular behavior more typical of resonant scattering, although the pattern is not on-resonance but somewhat displaced in E_0 from it. It could be due to the near-onset of the π_3* resonance (see Table 2). From our model this resonance for o-xylene is predicted at slightly lower E_0 (5.7 eV) than the others xylenes at 5.9 eV. However our ICSs show this resonance to be closer to the model values.

At the E_0 value of 5.0 eV the π_3* resonant behavior is weak (and broad, see Fig. 3) showing a slight maximum around $\theta = 90^o$ seen best in p-xylene (which has the largest cross section at this E_0 value, see Fig. 4). This weak maximum continues to E_0 = 10 eV. At the $E_0 \geq 5$ eV the DCSs for the three xylenes are almost identical and are about a factor of 1.7 higher than those of toluene indicating a geometric size factor ratio for these targets. Also, strong, similar forward scattering in these targets is indicative of the similar polarizabilities of these targets $\approx$ 16 $Å^3$ for xylene and $\approx$ 14 $Å^3$ [19]. Higher energy shape resonances are seen experimentally in the excitation functions in Fig. 3.Here p-xylene exhibits a single peak at $E_0 \approx$ 7.0 eV. However, o-xylene displays two peaks, a

higher one at $E_0 \approx 4.8$ eV and a weaker peak at $E_0 \approx 9.4$ eV and m-xylene also shows two similar, but weaker peaks at $E_0 \approx 5$ eV and at $E_0 \approx 9.0$ eV.

Our calculated ICSs and MTCSs presented in Fig. 4 show three shape resonances. In order to characterize those resonances we show in Fig. 6 the first three MVOs responsible for trapping the incident electron, and forming the resonances. Although the LUMO, LUMO+1 and LUMO+3 have almost identical shapes between the isomers, they present slight differences in energy, which in our model, reflects differences in the energy positions of negative ion resonances as shown in Table 2.

As mentioned before, is possible to observe three π^* shape resonances for each isomer (Fig. 4), and also a broad shoulder at 10 eV. The positions of the resonances are presented in Table 2. It is worth to mention that benzene has two π^* resonances located at 1.1 eV and 4.8 eV, the first being two fold degenerate and the second a mixture of shape and core-excited resonances [44]. Methylation of benzene to obtain the xylene isomers breaks the symmetry and lifts the degeneracy of the low-lying resonance of benzene. Despite the fact that for each isomer the resonances are located at different positions, figure 5 shows an interesting fact: each shape resonance presents distinct widths, which correspond to different lifetimes with respect to electron autodetachment. This is also observed for chlorophenol isomers [45], where the first two π^* shape resonances of meta-, para- and ortho-chlorophenol have small differences in position, but significant differences in width. For the xylene isomers, para-xylene presets the smallest width, corresponding to the longer lifetime, for the first resonance, while ortho-xylene present the smallest width for the second and third resonances.

IV. Conclusions

We have presented experimental and theoretical elastic DCSs, ICSs and MTCSs for low elastic energy electron scattering from the three xylene isomers at E_0 values ranging from 1 eV to 30 eV, which are large molecular mass targets. The three isomers were studied in order to investigate differences between these isomers for differential scattering by slow electrons. Except for our lowest E_0 values $\leq$ 5eV, we found the differential scattering cross section for these isomers to be essentially identical, and this, to some extent, supports the total photoionization results of Zhou et al. [10] who see the three isomers having similar photoionization cross sections. We observe that at these low E_0 values the role of the permanent dipole interaction dominates over the molecular polarizability, whereas at $E_0 \geq$ 5 eV molecular polarizability seems to be more important. The role of resonances differs in E_0 values (Table 2), and to some extent the experimental data indicates this behavior in Fig. 3. Unfortunately the present experimental work does not cover the region $E_0 \leq$ 1eV, which would confirm the sharpness and positions of the π_1^* resonances associated with the o-, m- and p- xylenes. This might be investigated by us in the near-future.

Ortho-, meta-, and para-xylene present three π^* shape resonances each, with small differences in their position between the isomers, but with significant differences in their width. We investigated the LUMO, LUMO+1 and LUMO+2 for each isomer to help in the characterization of the shape resonances, which present almost same shape.

V. Acknowledgements.

M. A. K. and L. R. H. acknowledge support from National Science Foundation Researchvia grants NSF-RUI-AMO 1306742 and 0968874. D. F. P. acknowledges support from Brazilian Agency Coordenação de Aperfeiçoamento de Pessoal de Nível Superior (CAPES). M.H.F.B. acknowledges support from Brazilian agencies Conselho Nacional de Desenvolvimento Científico e Tecnológico (CNPq), and Financiadora de Estudos e Projetos (FINEP), under project CTInfra. D. F. P. and M.H.F.B also acknowledge computational support from Professor Carlos M. de Carvalho at LFTC-DFis-UFPR and at LCPAD-UFPR, and from CENAPAD-SP.

VI. References

[1] B. Boudaïffa, P. Cloutier, D. Hunting, M. A. Huels and L. Sanche, Science, **287**, 1658 (2000).

[2] L. G. Christophorou, D. L. McCorkle and J. G. Garner, J. Chem. Phys. **60**, 3779 (1974).

[3] D. Mathur and J. B. Hasted, J. Phys. B: At. Mol. Phys. **9**, L31 (1976).

[4] S. L. Lunt, D. Field, S. V. Hoffmann, R. J. Gulley, and J-P. Ziesel, J. Phys. B **32**, 2707 (1999).

[5] J. K. Olthoff, J. A. Tossell, and J. H. Moore, J. Chem. Phys. **83**, 5627 (1985).

[6] A. Sakaamini, L. R. Hargreaves, M. A. Khakoo, D. F. Pastega, and M. H. F. Bettega, Phys. Rev. A **93**, 042704 (2016).

[7] H. Kato, M. C. Garcia, T. Asahina, M. Hoshino, C. Makochekanwa, and H. Tanaka, Phys. Rev. A **79**, 062703 (2009).

[8] H. Cho, R. J. Gulley, K. Sunohara, M. Kitajima, L. J. Uhlmann, H. Tanaka, and S. J. Buckman, J. Phys. B **34**, 1019 (2001).

[9] L. D. Moore, T. Le, and G. Fan, Neuropsychopharmacology Rev.**38**, 2338 (2013).

[10] Z. Zhou, M. Xie, Z. Wang and F. Qi, Rapid Comm. in Mass Spectrom. **23**, 3994 (2009).

[11] L. Chiari, A. Zecca, F. Blanco, G. García, and M. J. Brunger, J. Chem. Phys. **144**, 084301 (2016).

[12] K. Holste, W. Gärtner, P.R Köhler, P. Dietz, J. Konrad,S. Schippers, P. J. Klar, A. Müller and P. R. Schreiner, (*Proceedings of the Joint Conference of the 230th ISTS, 34th IEPC and 6th NSAT, Hyogo-Kobe, Japan, 2015*) IEPC-2015-320/ISTS-2015-b-320,

http://erps.spacegrant.org/uploads/images/2015Presentations/IEPC-2015-320_ISTS-2015-b-320.pdf .

[13] J. A. Barnard, B. M. Sankey, Combustion and Flame **12**, 353 (1968).

[14] Corina-Mihaela MANTA1, Ionut BANU2*, Georgeta BERCARU3, Grigore BOZGA, U.P.B. Sci. Bull., Series B**78**, 112 (2016).

[15] E. Yamamoto, T. Yoshidome, T. Ogawa and H. Kawazumi, J. Electr. Spectroscop. Rel. Phenomen. **63**, 341 (1993).

[16] I. G. Eustatiu, B. Huo, S. G. Urquhart and . P. Hitchcock, J. Electr. Spectroscop. Rel. Phenomen. **94**, 243 (1998).

[17] C. Q. Jiao and S. F. Adams, Chem. Phys. Letts. **573**, 24 (2013).

[18] A. G. Harrison, E. G. Jones, S. K. Gupta, G. P. Nagy, Can. J. Chem. **44**, 1967 (1966).

[19] J. Applequist, J. Phys. Chem. **97**, 6016 (1993).

[20] H. Kanai, V. Inouye, L. Yazawa, R. Goo, H. Wakatsuki, J. Chromatographic Sci. **43**, 57 (2005).

[21] M. A. Khakoo, C. E. Beckmann, S. Trajmar and G. Csanak, J. Phys. B **27**, 3159 (1994).

[22] ARi Industries Inc., Addison, IL 60101 USA, 1HN040B-16.3 biaxial cable.

[23] ETP Equipe Thermodynamique et Plasmas (ETP) model AF151.

[24] J. H. Brunt, G. C. King, and F. H. Read, J. Phys. B: At. Mol. Phys. **10**, 1289 (1977).

[25] M. A. Khakoo, K. Keane, C. Campbell, N. Guzman and K. Hazlett, J. Phys. B. **40**, 3601 (2007).

[26] M. Hughes, K. E. James, Jr., J. G. Childers, and M. A. Khakoo, Meas. Sci. Technol. **14**, 841 (1994).

[27] R. K. Nesbet, Phys. Rev. A **20**, 58 (1979).

[28] D. F. Register, S.Trajmar, and S. K. Srivastava, Phys. Rev. A **21**, 1134 (1980).

[29] MKS, Granville-Phillips Division, 6450 Dry Creek Parkway, Longmont, CO 80503 USA.

[30] K. Fedus, C. Navarro, L. R. Hargreaves, and M. A. Khakoo, F. M. Silva and M. H. F. Bettega, C. Winstead and V. McKoy, Phys. Rev. A **90**, 032708 (2014).

[31] K. Takatsuka and V. McKoy, Phys. Rev. A **24**, 2473 (1981); **30** 1734 (1984).

[32] M. H. F. Bettega, L. G. Ferreira, and M. A. P. Lima, Phys. Rev. A **47**, 1111 (1993).

[33] J. S. dos Santos, R. F. da Costa, and M. T. do N. Varella, J. Chem. Phys. **136**, 084307 (2012).

[34] R. F. da Costa, M. T. do N. Varella, M. H. F. Bettega, and M. A. P. Lima, Eur. Phys. J. D **69**, 159 (2015).

[35] M. W. Schimidt, K. K. Baldridge, J. A. Boatz, S. T. Elbert, M.S. Gordon, J. H. Jensen, S. Koeseki, N. Matsunaga, K. A. Nguyen, S. J. Su, T. L. Windus, M. Dupuis, and J. A. Montgomery, J. Comput. Chem. **14**, 1347 (1993).

[36] R. Disselkamp, E. R. Bernstein, J. I. Seeman, and H. V. Secor, J. Chem. Phys. **97**, 11 (1992).

[37] M. H. F. Bettega, A. P. P. Natalense, M. A. P. Lima, and L. G. Ferreira, Int. J. Quantum Chem. **60**, 821 (1996).

[38] G. B. Bachelet, D. R. Hamann, and M. Schlüter, Phys. Rev. B **26**, 4199 (1982).

[39] T. H. Dunning Jr., J. Chem. Phys. **53**, 2823 (1970).

[40] C. W. Bauschlicher Jr., J. Chem. Phys **72**, 880 (1980).

[41] E. M. de Oliveira, M. T. do N. Varella, M. H. F. Bettega, and M. A. P. Lima, Eur. Phys. J. D **68**, 65 (2014).

[42] N. K. Sanyal, P. Ahmad, and L. Dixit, J. Phys. Chem. **77**, 2552 (1973).

[43] See http://openmopac.net/Polarizability_table.html.

[44] I. Nenner and G. J. Schulz, J. Chem. Phys. **62**, (1975).

[45] F. Kossoski and M. T. do N. Varella, J. Chem. Phys. **145**, 044310 (2016).

VII. Tables and Figures

θ (deg)	1 eV	Error	1.5 eV	Error	2 eV	Error	3 eV	Error	5 eV	Error	10 eV	Error	15 eV	Error	20 eV	Error	30 eV	Error
10											96.0	12.2	132	17	142	17	133	17
15									43.6	5.6	76.4	9.2	83.9	10.4	74.3	9.1	54.0	3.6
20					11.3	1.4	14.2	1.9	32.5	4.0	51.0	6.0	44.3	5.0	35.0	4.2	18.2	1.1
25	11.8	1.6	10.9	1.6	8.52	1.16	10.7	1.4	23.5	3.0			22.3	2.7	15.0	1.8	9.06	1.16
30	8.60	1.20	8.39	1.11	6.72	0.85	10.6	1.4	18.4	2.2	17.4	2.0	11.9	1.3	8.48	1.07	5.84	0.41
35	6.05	0.84	6.82	0.89														
40	4.89	0.67	6.66	0.84	6.64	0.79	11.2	1.4	12.6	1.6	8.13	0.93	5.22	0.62	4.48	0.52	3.01	0.23
50	4.28	0.60	6.07	0.78	7.04	0.85	10.8	1.4	9.36	1.21	5.13	0.59	3.66	0.42	2.90	0.34	2.36	0.24
60	5.28	0.74	6.10	0.76	6.48	0.77	8.47	1.02	5.72	0.69	4.15	0.51	2.81	0.32	2.64	0.32	2.05	0.11
70	6.04	0.75	5.42	0.66	5.34	0.69	6.33	0.77	4.58	0.57	3.85	0.46	2.71	0.32	2.59	0.31	1.58	0.27
80	6.29	0.80	4.64	0.57	4.00	0.49	4.49	0.57	4.39	0.56	3.84	0.43	2.50	0.28	2.08	0.25	1.21	0.11
90	5.94	0.78	3.74	0.48	3.02	0.36	4.06	0.49	4.47	0.56	4.10	0.50	2.24	0.26	1.91	0.22	1.11	0.11
100	5.39	0.71	3.08	0.38	2.41	0.33	4.16	0.50	4.12	0.53	4.04	0.49	2.19	0.25	1.83	0.21	1.05	0.06
110	4.84	0.66	2.90	0.38	2.94	0.36	4.19	0.50	3.54	0.45	3.72	0.44	2.28	0.26	1.91	0.22	1.29	0.07
120	4.35	0.58	3.15	0.39	3.56	0.46	4.05	0.52	3.40	0.42	3.60	0.41	2.68	0.30	2.08	0.25	1.57	0.11
125	4.48	0.58			3.83	0.52	3.83	0.47	3.56	0.43	3.68	0.43						
130			3.25	0.44			3.64	0.52	3.89	0.50	3.88	0.45	3.22	0.37	2.53	0.32	1.70	0.16
ICS	75.2	11.1	67.2	9.3	63.3	8.1	79.6	10.0	91.8	11.4	98.7	9.1	87.6	10.1	79.9	9.4	65.6	6.5
MTCS	66.0	9.7	52.7	7.3	51.9	6.7	59.6	7.5	56.6	7.0	53.3	4.9	43.7	5.1	33.0	3.9	20.5	2.0

Table 1a. o-xylene

θ (deg)	1 eV	Error	1.125 eV	Error	1.5 eV	Error	2 eV	Error	3 eV	Error	5 eV	Error	10 eV	Error	15 eV	Error	20 eV	Error	30 eV	Error
10													94.7	11.7	118	14	114	15	148	18
15									17.5	2.4	50.6	7.0	70.0	8.1	65.7	7.9	72.1	9.0	53.3	6.1
20							9.30	1.17	11.76	1.53	31.8	3.9	45.0	5.2	38.2	4.8	34.8	4.4	20.2	2.2
25	13.9	1.7	14.4	1.9	11.8	1.5	7.39	0.90	9.17	1.10							15.5	2.0	9.67	1.12
30.0	10.4	1.2	10.3	1.3	9.55	1.12	6.76	0.78	7.94	0.92	17.3	2.0	15.7	1.9	10.0	1.8	9.12	1.12	5.74	0.65
40	4.89	0.64	6.08	0.77	7.75	0.95	6.88	0.81	7.95	0.95	11.43	1.38	7.03	0.87	5.38	1.06	3.97	0.50	2.55	0.29
50	2.93	0.36	4.52	0.54	7.22	0.87	7.11	0.87	7.44	0.87	8.31	1.03	4.55	0.58	3.68	0.56	2.55	0.33	1.88	0.22
60	3.43	0.43	4.22	0.52	6.98	0.84	5.84	0.74	5.55	0.68	5.41	0.64	3.61	0.46	2.86	0.40	2.21	0.27	1.57	0.18
70	4.48	0.50	4.70	0.54	6.14	0.74	4.11	0.50	3.82	0.46	4.37	0.53	3.45	0.44	2.56	0.37	2.04	0.25	1.32	0.15
80	5.37	0.71	5.17	0.64	5.12	0.61	2.88	0.36	2.81	0.34	4.23	0.52	3.14	0.40	2.35	0.32	1.72	0.22	0.969	0.114
90	5.13	0.67	4.71	0.55	3.92	0.49	2.33	0.28	2.23	0.26	3.65	0.44	3.31	0.40	2.12	0.28	1.36	0.17	0.926	0.107
100	4.60	0.58	3.94	0.49	3.35	0.41	1.94	0.24	2.09	0.24	3.31	0.39	3.25	0.40	1.91	0.25	1.28	0.16	0.923	0.108
110	4.16	0.45	3.61	0.46	3.15	0.38	2.02	0.24	2.27	0.27	3.34	0.42	2.92	0.36	2.00	0.25	1.47	0.18	0.971	0.115
120	4.17	0.51	3.34	0.43	3.24	0.39	2.15	0.26	2.18	0.27	3.70	0.49	2.57	0.33	2.40	0.30	1.59	0.20	1.20	0.14
125	4.41	0.51	3.11	0.41	3.53	0.45	2.14	0.27	2.28	0.27	3.93	0.53	2.52	0.31	2.87	0.36				
130											4.16	0.50	2.56	0.32	2.91	0.39	1.91	0.24	1.46	0.17
ICS	74.0	10.4	70.7	10.2	73.5	10.3	54.7	7.7	57.5	7.9	92.4	10.4	86.6	9.1	80.0	9.6	70.0	10.0	62.7	8.4
MTCS	64.4	9.1	50.7	7.3	54.3	7.6	38.3	6.0	39.8	5.5	56.8	6.4	41.8	4.4	37.1	4.5	26.7	3.8	20.0	2.7

Table 1b. m-xylene

θ (deg)	1 eV	Error	1.5 eV	Error	2 eV	Error	3 eV	Error	5 eV	Error	10 eV	Error	15 eV	Error	20 eV	Error	30 eV	Error
10											160	24	134	20	206	29	142	19
15									47.1	6.7	100.4	12.5	82.5	10.8	96.4	12.8	67.1	9.0
20					12.8	1.7	18.7	2.8	31.6	4.4	63.9	8.2	46.9	6.1	45.5	5.7	25.0	3.3
25	6.71	0.86	12.08	1.77	10.7	1.3	12.6	1.8	20.5	2.5					22.5	2.8	11.6	1.4
30	5.09	0.63	9.24	1.39	9.55	1.22	11.9	1.5	14.6	1.8	24.4	3.1	15.0	1.9	12.3	1.6	5.98	0.72
35	5.15		7.51	0.98														
40	5.23	0.70	7.34	0.98	9.15	1.21	10.2	1.2	11.6	1.4	10.5	1.3	5.59	0.71	4.56	0.58	3.33	0.42
50	6.04	0.75	6.69	0.85	8.24	1.03	8.43	1.04	8.65	1.06	5.90	0.76	4.11	0.53	4.01	0.51	2.21	0.27
60	5.96	0.76	6.71	0.84	6.28	0.80	6.01	0.73	5.99	0.76	4.47	0.54	3.84	0.48	2.99	0.38	1.78	0.23
70	7.20	0.92	5.97	0.72	4.95	0.63	4.30	0.52	4.45	0.56	4.42	0.54	2.89	0.35	2.80	0.36	1.59	0.19
80	6.84	0.84	5.11	0.63	3.61	0.44	3.37	0.41	4.17	0.53	4.50	0.54	2.65	0.33	2.47	0.31	1.19	0.15
90	7.16	0.99	4.12	0.53	2.61	0.34	2.33	0.28	4.27	0.54	4.03	0.51	2.55	0.32	2.02	0.25	1.03	0.13
100	7.48	1.02	3.39	0.43	2.01	0.25	1.95	0.25	3.98	0.50	4.12	0.51	2.26	0.29	1.80	0.22	1.01	0.12
110	7.48	1.00	3.20	0.40	1.92	0.24	1.89	0.24	3.75	0.48	3.95	0.50	2.27	0.29	1.96	0.25	1.14	0.14
120	7.46	0.98	3.47	0.47	2.75	0.35	2.12	0.26	4.11	0.51	3.71	0.46	2.65	0.34	2.32	0.30	1.32	0.17
125	7.69	0.97			3.61	0.46	2.18	0.27	4.33	0.53	3.56	0.45						
130			3.58	0.47							3.48	0.46	3.22	0.40	2.82	0.38	1.70	0.21
ICS	89.5	11.4	71.8	9.0	71.5	9.5	69.6	9.4	98.6	13.3	128	14	97.3	11.1	105	14	75.4	10.4
MTCS	92.8	11.8	54.7	6.9	60.3	8.0	44.8	6.1	67.3	9.1	56.5	6.3	43.7	5.0	41.3	5.6	25.9	3.6

Table 1c. p-xylene

Tables 1 (a – c): DCSs, ICSs and MTCSs for elastic scattering of electrons from o- m- and p-xylene. DCS are in 10^{-16} cm^2/sr units. ICS and MTCS are in 10^{-16} cm^2 units. Errors are 1 standard deviation.

	π_1^*	π_2^*	π_3^*
o-xylene	1.10	1.15	5.7
m-xylene	1.00	1.15	5.9
p-xylene	0.78	1.23	5.9

Table 2: Positions (in eV) of the shape resonances of o-xylene, m-xylene and p-xylene.

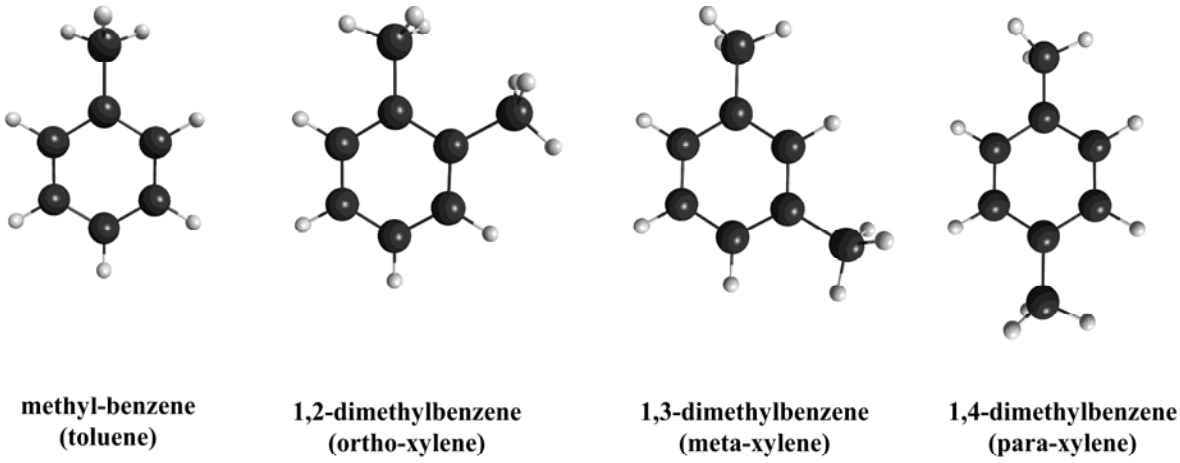

Figure 1a: Ball and stick models of toluene, o-, m- and p- xylenes.

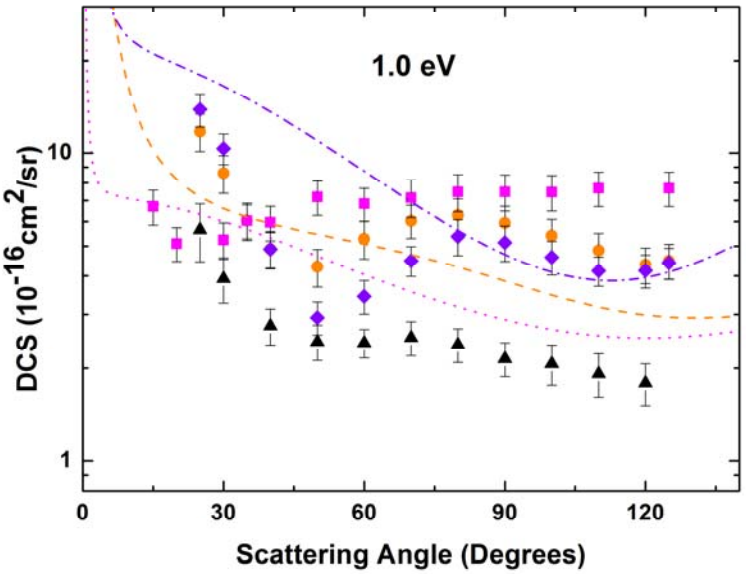
1.0 eV
DCS (10^{-16}cm^2/sr)
10
1
0
30
60
90
120
Scattering Angle (Degrees)

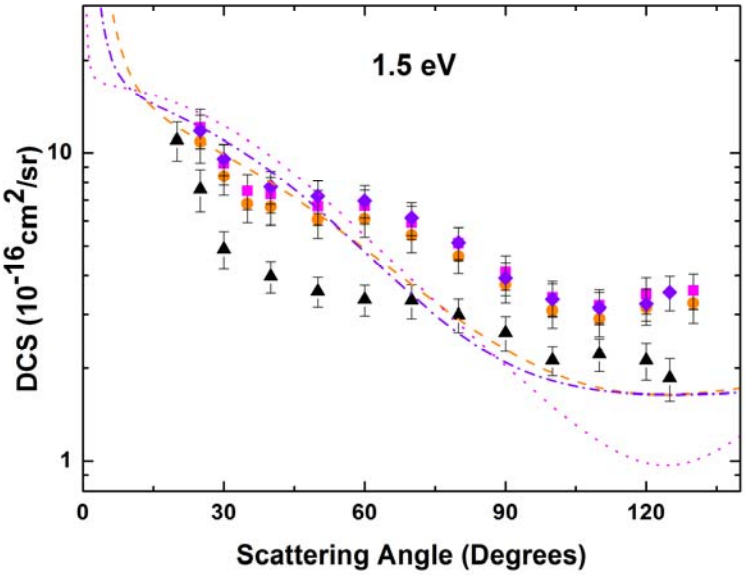
1.5 eV
DCS (10^{-16}cm^2/sr)
10
1
0
30
60
90
120
Scattering Angle (Degrees)

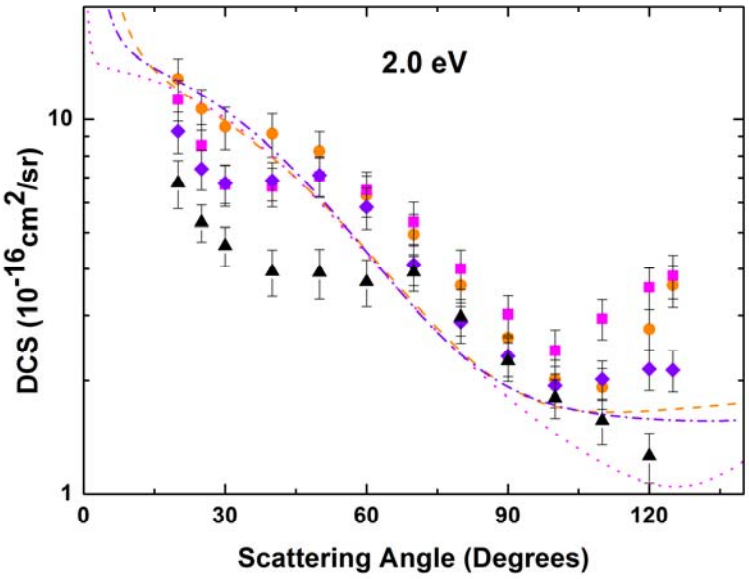
2.0 eV
DCS (10^{-16}cm^2/sr)
10
1
0
30
60
90
120
Scattering Angle (Degrees)

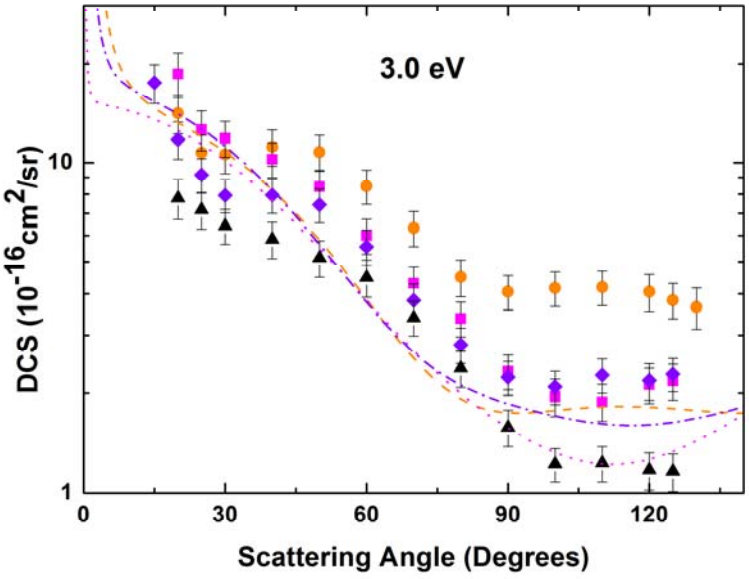
3.0 eV
DCS (10^{-16}cm^2/sr)
10
1
0
30
60
90
120
Scattering Angle (Degrees)

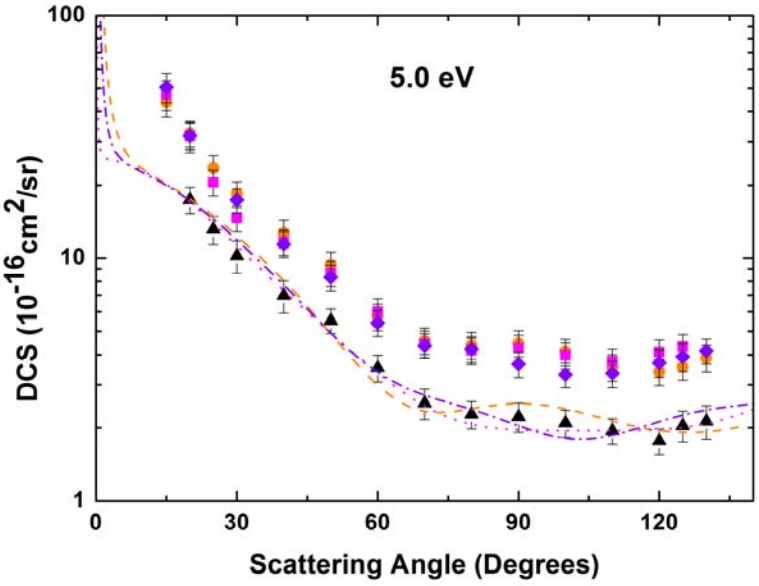
5.0 eV
DCS (10^{-16}cm^2/sr)
Scattering Angle (Degrees)
100
10
1
0
30
60
90
120

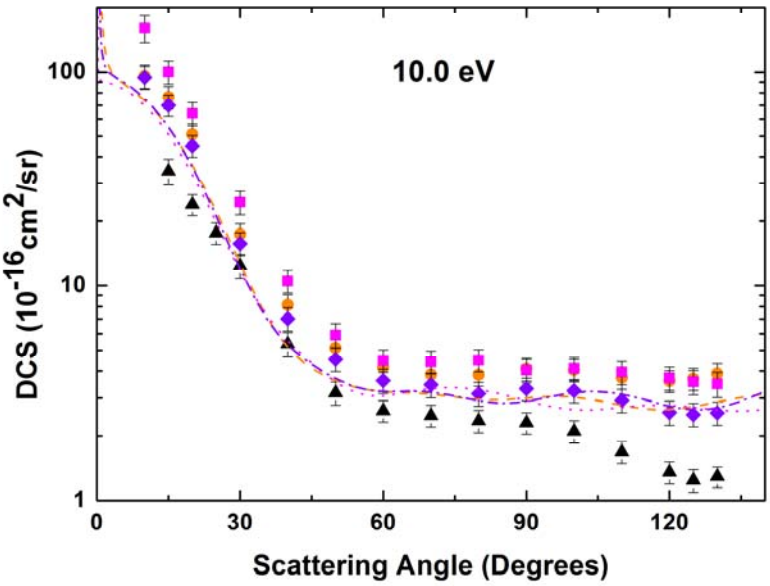
10.0 eV
DCS (10^{-16}cm^2/sr)
Scattering Angle (Degrees)
100
10
1
0
30
60
90
120

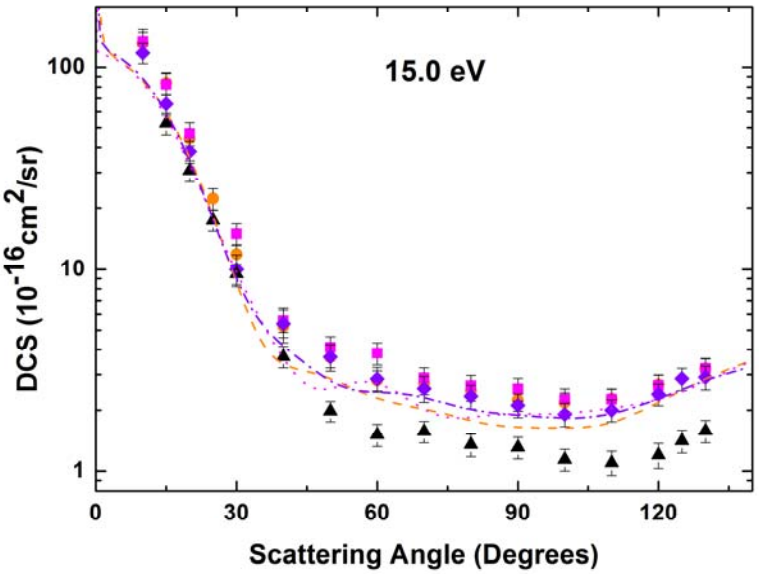
15.0 eV
DCS (10^{-16}cm^2/sr)
100
10
1
0
30
60
90
120
Scattering Angle (Degrees)

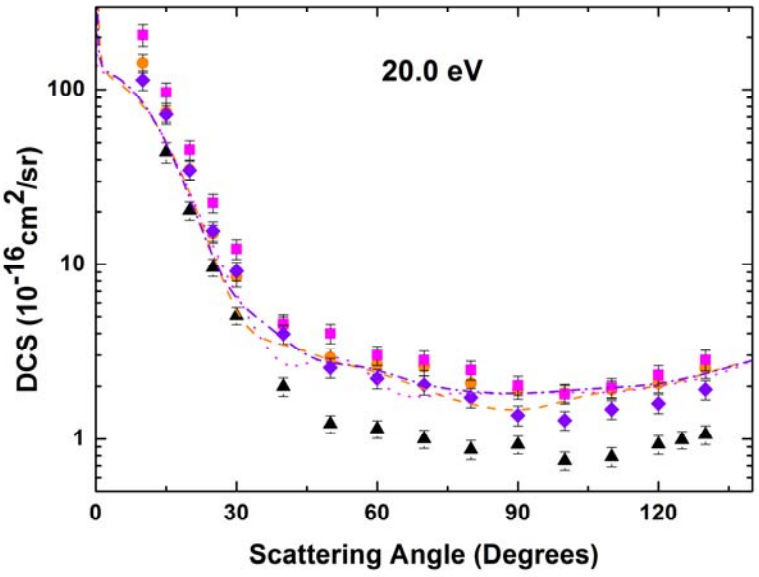
20.0 eV
DCS (10^{-16}cm^2/sr)
100
10
1
0
30
60
90
120
Scattering Angle (Degrees)

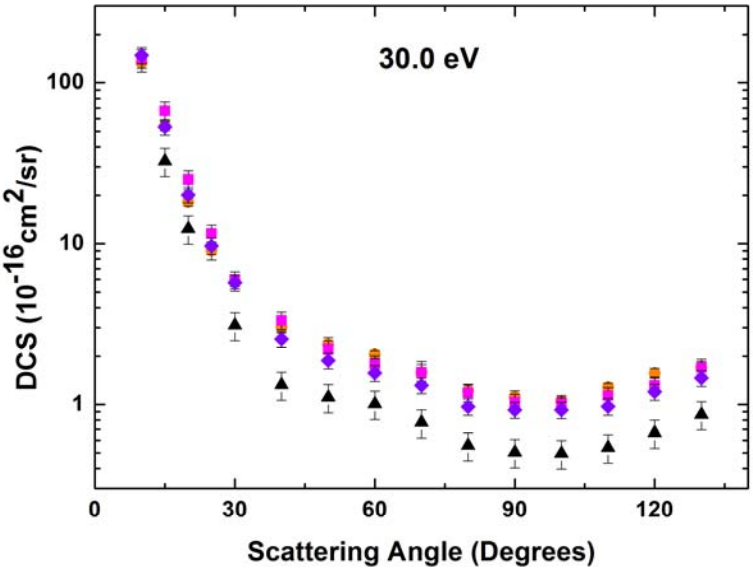

Figure 2 (Color online): DCSs for elastic electron scattering from o-, m- and p- xylenes. Legend: Present experiment: ● o-xylene, ♦ m-xylene, ■ p-xylene, ▲toluene (except reference [6] at $E_0 = 30$eV); Theory: Schwinger multi-channel —o-xylene, — - —m-xylene, ------ p-xylene.

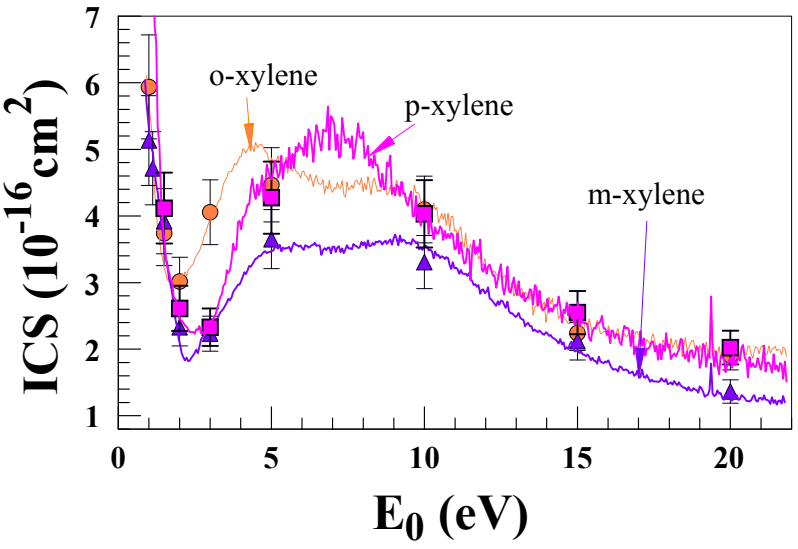

Figure 3 (Color online):DCSs for elastic electron scattering from o-, m- and p- xylenes at θ = 90^o as a function of E_0 (excitation functions): legend: orange line, o-xylene; magenta line, m-xylene; pink line, p-xylene and present experimental DCSs at 90^o from Table 2: legend: ● o-xylene, ♦ m-xylene, ■ p-xylene.The "spikes" at E_0 = 19.33 eV are due to the elastic scattering He^- 2^2S resonance which produces a sharp dip at this incident electron energy. He elastic scattering excitation functions are taken serially with the xylene excitation functions, are used to normalize the excitation functions using data from [26] and also calibrate E_0 in the measurements using the He^- 2^2S resonance energy from [24].

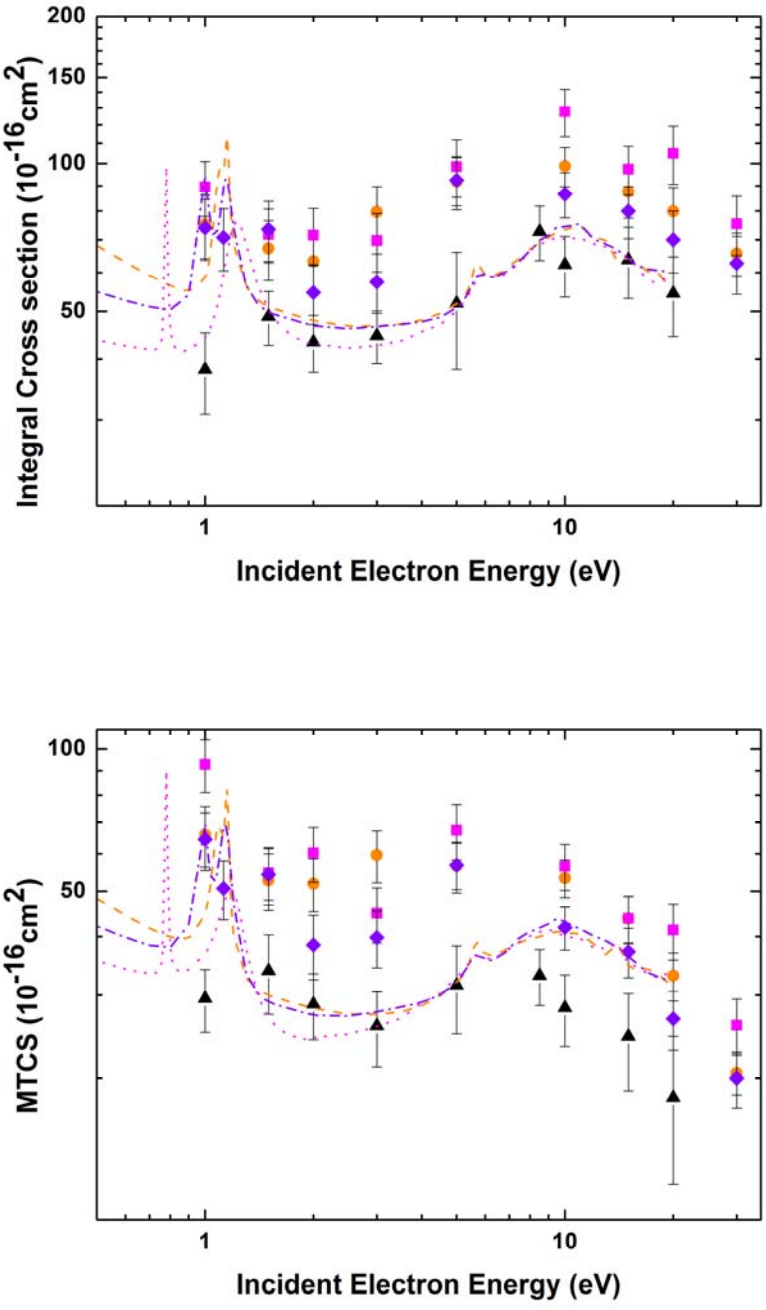

Figure 4 (Color online):ICSs and MTCSs for elastic electron scattering from o, m and p xylenes. Legend: Present experiment: ● o-xylene, ♦ m-xylene, ■ p-xylene, ▲ toluene (Note: at E_0 = 30eV DCSs are from [7]); Theory: Schwinger multi-channel —o-xylene, — - —m-xylene, ----- p-xylene.

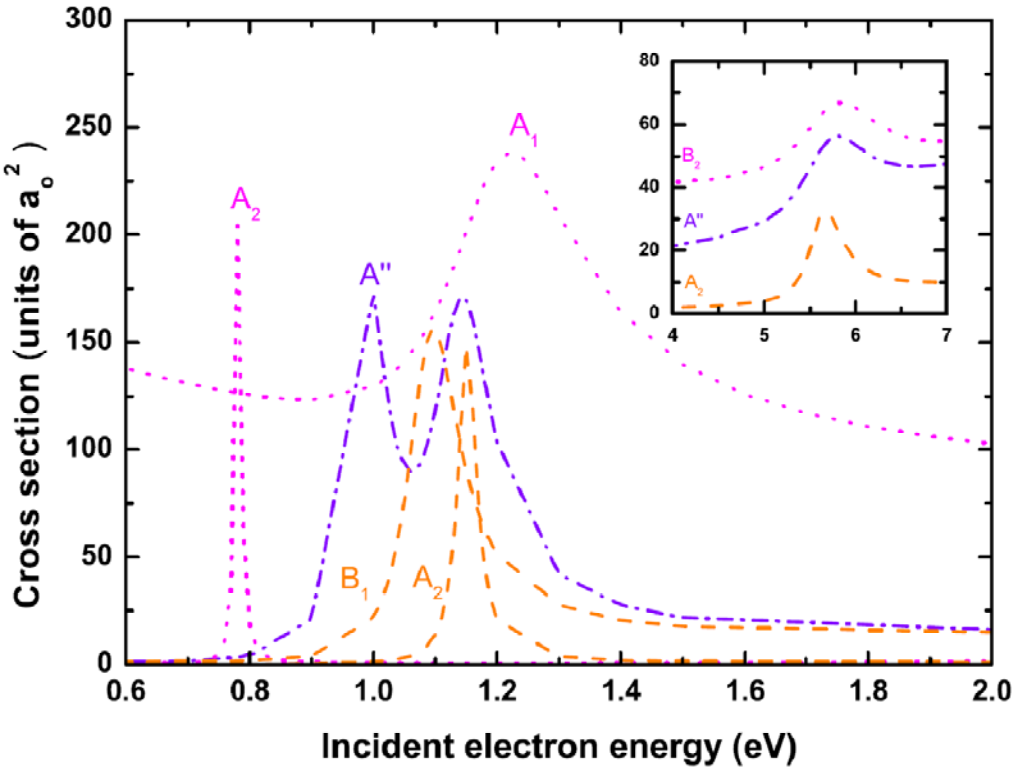

Figure 5 (Color online): Calculated symmetry decomposition of the ICS into partial CSs for the resonant irreducible representation. Legend: o-xylene resonant symmetries (orange dash line); m-xylene resonant symmetry (magenta dot-dash line); p-xylene resonant symmetries (pink dotted line).

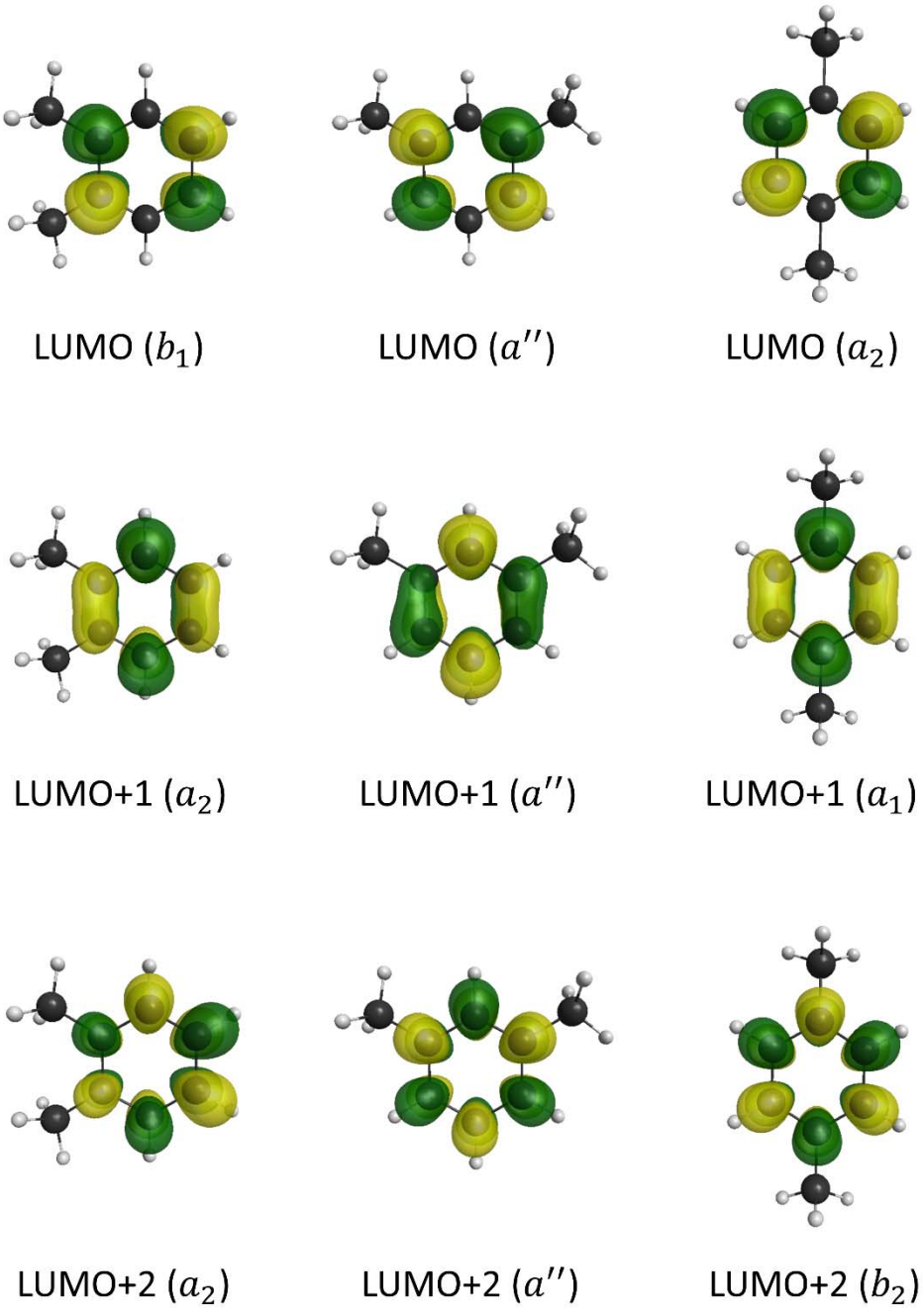

Figure 6 (Color online): Resonant orbitals of xylenes and its symmetries. Ortho-xylene on the left, m-xylene in the middle and p-xylene on the right. at first row, at the second row and at the third row.